Electron-impact ionization of Ar^{7+}

S. S. Tayal
Department of Physics and Center for Theoretical Studies of Physical Systems, Clark Atlanta University, Atlanta, Georgia 30314
(Received 20 September 1993; revised manuscript received 12 November 1993)

Cross sections for the ionization of Ar^{7+} by electron impact have been calculated using the R-matrix method in two independent 19- and 45-state close-coupling approximations. Autoionization states arising from the $2s^22p^53s3l$ configurations together with the ground and excited $2s^22p^63l$ states are included in the close-coupling expansion in the 19-state calculation, while additional autoionization states arising from the $2s^22p^53s4l$ ($l=0,1,2$) and $2s2p^63s3l$ configurations and the low-lying bound states $2s^22p^64l$ are also included in the 45-state calculation. Several Rydberg series of resonances converging to various autoionizing states are formed due to the resonant-excitation-double-autoionization process and these are found to significantly enhance the cross sections in the autoionizing threshold region. The calculated results are compared with the recent crossed-beam measurements.

PACS number(s): 34.80.Dp

I. INTRODUCTION

Electron-impact ionization cross sections of ions are needed in the modeling and diagnostics of laboratory and astrophysical plasmas. The importance of indirect physical mechanisms of ionization is now well recognized. In many cases the indirect-ionization processes dominate the cross sections over a wide energy range and their importance over the direct ionization increases with increasing ionic charge along the isoelectronic sequence. Excitation-autoionization (EA) and resonant-excitation-double-autoionization (REDA) processes are the most important indirect-ionization processes in the electron-impact ionization of positive ions. In the EA process an inner-shell electron is excited to a level above the ionization threshold which can subsequently decay by autoionization. The EA process can cause a substantial increase in the ionization cross sections close to the excitation thresholds. The REDA process is a resonant process that occurs when the incident electron is captured temporarily with simultaneous excitation of an inner-shell electron to form the doubly excited states which can decay by successive emission of two electrons. The REDA process gives rise to Rydberg series of resonances converging to excitation thresholds.

Na-like ions have received considerable theoretical and experimental attention in recent years because of their simple atomic structure. The REDA process was first postulated by LaGattuta and Hahn [1] in connection with the electron-impact ionization of Na-like Fe^{15+}. Tayal and Henry [2] and Chen, Reed, and Moores [3] calculated REDA cross sections for the Na-like Fe^{15+} ions using the R-matrix method [4] and a multiconfiguration Dirac-Fock model, respectively. Gregory *et al.* [5] reported measured absolute cross sections for electron-impact ionization of Fe^{15+}. Chen, Reed, and Moores [3] found that the contribution of the REDA process to the total ionization cross sections of Fe^{15+} is about 30%. Muller *et al.* [6] and Peart, Thomason, and Dolder [7] emphasized the importance of indirect processes in their measurements on electron-impact ionization of Na-like Mg^+. Tayal [8] calculated the contributions of the EA and REDA indirect-ionization mechanisms to electron-impact ionization of Mg^+. Recently, Zhang *et al.* [9] and Rachafi *et al.* [10] reported absolute cross-section measurement of electron-impact ionization of Na-like Ar^{7+} using the crossed-beam techniques. They predicted a significant contribution due to the indirect processes to the cross sections. It is difficult to resolve the fine resonance structure due to the REDA process in the experiment and it depends critically on the energy resolution of a particular experiment. Muller *et al.* [6] and Peart, Thomason, and Dolder [7] in their high-resolution experiments on Mg^+, which is isoelectronic to Ar^{7+}, provided clearcut evidence for the existence of resonance structure due to the REDA process. In this paper we present our calculation of EA and REDA contributions to the electron-impact ionization of Ar^{7+}. Our calculation clearly demonstrates the importance of both EA and REDA indirect-ionization processes.

Earlier, the contribution of the indirect-ionization processes to the total ionization cross sections of sodiumlike ions had been considered by Moores and Nussbaumer [11] in the Coulomb-Born approximation and by Cowan and Mann [12] and Griffin *et al.* [13,14] in the distorted-wave approximations. Henry and Msezane [15] employed a close-coupling approach to calculate electron-impact ionization cross sections for Mg^+, Al^{2+}, and Si^{3+}. On the experimental front, Crandall *et al.* [16] measured absolute ionization cross sections for Mg^+, Al^{2+}, and Si^{3+}. Donets and Ovsyannikov [17] have given the ionization cross sections for Ar^{7+} at 2500 eV. Younger [18] calculated direct-ionization cross sections for Na-like ions using the distorted-wave–Born-exchange approximation.

II. CALCULATION

We consider EA reactions of the type where a $2p$ electron is excited into a nl ($n=3,4$; $l=0,1,2$) orbital:

$$e^- + \mathrm{Ar}^{7+}(2s^2 2p^6 3s) \rightarrow \mathrm{Ar}^{7+*}(2s^2 2p^5 3snl) + e^- , \quad (1)$$

followed by the autoionization

$$e^- + \mathrm{Ar}^{7+*}(2s^2 2p^5 3snl) \rightarrow \mathrm{Ar}^{8+}(2s^2 2p^6) + e^- , \quad (2)$$

or a $2s$ electron is excited into the $n=3$ shell:

$$e^- + \mathrm{Ar}^{7+}(2s^2 2p^6 3s) \rightarrow \mathrm{Ar}^{7+*}(2s 2p^6 3snl) + e^- , \quad (3)$$

followed by the autoionization

$$\mathrm{Ar}^{7+*}(2s 2p^6 3snl) \rightarrow \mathrm{Ar}^{8+}(2s^2 2p^6) + e^- , \quad (4)$$

and the REDA ionizing process of the type where the incident electron is captured into a resonant state,

$$e^- + \mathrm{Ar}^{7+}(2s^2 2p^6 3s) \rightarrow \mathrm{Ar}^{6+*}(2s^2 2p^5 3snln'l') \quad (5)$$

and

$$e^- + \mathrm{Ar}^{7+}(2s^2 2p^6 3s) \rightarrow \mathrm{Ar}^{6+*}(2s 2p^6 3snln'l') , \quad (6)$$

followed by sequential double autoionization,

$$\mathrm{Ar}^{6+*}(2s^2 2p^5 3snln'l') \rightarrow \mathrm{Ar}^{7+*}(2s^2 2p^5 3snl) + e^- \quad (7)$$

$$\rightarrow \mathrm{Ar}^{8+}(2s^2 2p^6) + e^- \quad (8)$$

and

$$\mathrm{Ar}^{6+*}(2s 2p^6 3snln'l') \rightarrow \mathrm{Ar}^{7+*}(2s^2 p^6 3snl) + e^- \quad (9)$$

$$\rightarrow \mathrm{Ar}^{8+}(2s^2 2p^6) + e^- . \quad (10)$$

We included the ground $2s^2 2p^6 3s\ ^2S$ and excited $2s^2 2p^6 3p\ ^2P^o$ and $2s^2 2p^6 3d\ ^2D$ states together with the important autoionizing states arising from the $2s^2 2p^5 3s^2$, $2s^2 2p^5 3s 3p$, and $2s^2 2p^5 3s 3d$ configurations in our 19-state calculation. Thus, the 19-state calculation includes the $2s^2 2p^5 3s 3lnl'$ Rydberg series of resonances converging to the $2s^2 2p^5 3s 3l$ autoionizing thresholds. There are many other possible autoionizing states which may contribute to the indirect EA and REDA processes. The doubly excited states formed as a first step in the REDA process [Eqs. (5) and (6)] can decay to singly excited bound states and thus will not contribute to the ionization process. Chen, Reed, and Moores [3] have reported that the $2s^2 2p^5 3s 4l 4l'$ and $2s 2p^6 3s 3lnl'$ resonances make the most important contributions to the REDA for electron-impact ionization of isoelectronic Fe^{15+}. In order to investigate the importance of these resonances for Ar^{7+} and also to allow for the loss of flux due to the decay of doubly excited states to the singly excited $2s^2 2p^6 4l$ bound states, we carried out an independent 45-state calculation. In addition to the states considered in the 19-state calculation, we also included $2s^2 2p^6 4l$ bound states and important autoionizing states arising from the $2s^2 2p^5 3snl$ ($n=4$; $l=0,1,2$) and $2s 2p^6 3s 3l$ configurations in the 45-state calculation. The ionic states are represented by configuration-interaction (CI) wave functions constructed from the ten orthogonal one-electron orbitals: $1s$, $2s$, $2p$, $3s$, $3p$, $3d$, $4s$, $4p$, $4d$, and $4f$. The $1s$, $2s$, and $2p$ orbitals are taken from Clementi and Roetti [19]. The $3s$ radial function is optimized on the combination of the $2s^2 2p^6 3s\ ^2S$ and the $2s^2 2p^5 3s 3p\ ^2S$ states, while $3p$ and $3d$ orbitals are chosen to improve the energies of the $2s^2 2p^5 3s 3p\ ^2S$ and $2s^2 2p^5 3s 3d\ ^2P^o$ states, respectively [20]. The $4s$, $4p$, and $4d$ orbitals are optimized on the combination of the

$$2s^2 2p^5 3s(^{3,1}P^o) 4s\ ^2P^o ,$$

$$2s^2 2p^5 3s(^{3,1}P^o) 4p\ ^2S ,$$

and

$$2s^2 2p^5 3s(^{3,1}P^o) 4d\ ^2P^o$$

states, respectively. The function $4f$ is optimized on the $2s^2 2p^6 4f\ ^2F^o$ state. In Table I we give the parameters of the Slater-type orbitals for the $3s$, $3p$, $3d$, $4s$, $4p$, $4d$, and $4f$ functions. The calculated excitation energies in eV relative to the ground $2s^2 2p^6 3s\ ^2S$ state are given in Table II.

The total wave function representing the electron-ion collision is expanded in terms of the N-electron target wave functions and $(N+1)$-electron bound-state-type functions ϕ_j by the close-coupling expansion

$$\Psi_k = A \sum_{ij} c_{ijk} \Phi_i(1,2,\ldots,11;\hat{\mathbf{r}}_{12}\sigma_{12}) u_{ij}(r_{12}) r_{12}^{-1} + \sum_j d_{jk} \phi_j(1,2,\ldots,12) , \quad (11)$$

where A is the antisymmetrization operator, the Φ_i are channel functions formed by coupling the spin and angular functions of the scattered electron with the target-state wave functions, and the u_{ij} are the numerical basis

TABLE I. Parameters of the bound orbitals used in the calculation. Each orbital is the sum of Slater-type orbitals.

Orbital	Coefficient	Power of r	Exponent
$3s$	−0.108 84	1	18.148 40
	−0.002 01	1	28.223 50
	0.467 10	2	6.897 20
	−0.061 71	2	16.275 20
	−1.250 88	3	3.394 15
	0.253 09	3	5.899 54
$3p$	0.386 53	2	6.282 96
	0.050 24	2	12.073 84
	0.714 40	3	3.968 01
	−1.593 08	3	3.454 17
	−0.189 11	3	2.666 89
$3d$	0.044 49	3	7.212 09
	0.573 42	3	3.268 06
	0.413 77	3	2.592 52
$4s$	0.104 94	1	13.997 43
	−0.448 37	2	5.867 40
	1.583 21	3	2.923 31
	−1.860 84	4	2.376 78
$4p$	0.265 96	2	6.932 76
	−4.111 33	3	1.875 41
	4.714 01	4	2.139 96
$4d$	0.753 21	3	3.153 95
	−1.215 56	4	1.917 12
$4f$	1.000 00	4	2.008 82

functions describing the radial motion of the scattered electron. The coefficients c_{ijk} and d_{jk} are determined by diagonalizing the total Hamiltonian of the $(N+1)$-electron system. The application of a variational principle leads to a set of coupled integro-differential equations which are solved numerically by the R-matrix method [4]. At each electron energy, cross sections are obtained for angular momenta $L=0$–20. These partial waves give converged cross sections for all the transitions over a wide range of energies considered in this work.

The total ionization cross sections can be assumed as the sum of direct- and indirect-ionization cross sections, if the interference effect is ignored. The cross sections for the direct ionization of the 3s, 2p, and 2s subshells are obtained from Younger's parameters for Na-like ions [18]. The indirect cross sections for the EA and REDA processes may depend on branching ratios at each step in Eqs. (4), (7), and (8). We have ignored radiative decay of the autoionizing states in the present work and thus assumed the branching ratios to be unity.

TABLE II. Excitation energies (eV) of the autoionizing states relative to the ground $2p^6 3s\ ^2S$ state.

Key	State	Energy
1	$2s^2 2p^6 3s\ ^2S$	0.0
2	$2s^2 2p^5 3s^2\ ^2P^o$	248.63
3	$2s^2 2p^5 3s(^3P^o)3p\ ^4S$	258.27
4	$2s^2 2p^5 3s(^3P^o)3p\ ^4D$	260.41
5	$2s^2 2p^5 3s(^3P^o)3p\ ^4P$	261.95
6	$2s^2 2p^5 3s(^1P^o)3p\ ^2D$	262.60
7	$2s^2 2p^5 3s(^1P^o)3p\ ^2P$	263.15
8	$2s^2 2p^5 3s(^1P^o)3p\ ^2S$	264.60
9	$2s^2 2p^5 3s(^3P^o)3p\ ^2D$	270.66
10	$2s^2 2p^5 3s(^3P^o)3p\ ^2P$	271.92
11	$2s^2 2p^5 3s(^3P^o)3p\ ^2S$	276.26
12	$2s^2 2p^5 3s(^3P^o)3d\ ^4P^o$	285.97
13	$2s^2 2p^5 3s(^3P^o)3d\ ^4F^o$	286.91
14	$2s^2 2p^5 3s(^3P^o)3d\ ^4D^o$	288.59
15	$2s^2 2p^5 3s(^1P^o)3d\ ^2P^o$	289.80
16	$2s^2 2p^5 3s(^3P^o)3d\ ^2P^o$	294.09
17	$2s^2 2p^5 3s(^3P^o)4s\ ^4P^o$	322.36
18	$2s^2 2p^5 3s(^3P^o)4s\ ^2P^o$	323.86
19	$2s2p^6 3s^2\ ^2S$	324.26
20	$2s^2 2p^5 3s(^1P^o)4s\ ^2P^o$	325.36
21	$2s^2 2p^5 3s(^3P^o)4p\ ^4S$	329.07
22	$2s^2 2p^5 3s(^3P^o)4p\ ^4D$	329.65
23	$2s^2 2p^5 3s(^3P^o)4p\ ^4P$	330.07
24	$2s^2 2p^5 3s(^3P^o)4p\ ^2D$	330.44
25	$2s^2 2p^5 3s(^3P^o)4p\ ^2P$	330.57
26	$2s^2 2p^5 3s(^1P^o)4p\ ^2S$	331.57
27	$2s^2 2p^5 3s(^1P^o)4p\ ^2D$	331.63
28	$2s^2 2p^5 3s(^1P^o)4p\ ^2P$	332.03
29	$2s^2 2p^5 3s(^3P^o)4p\ ^2S$	334.35
30	$2s^2 2p^5 3s(^3P^o)4d\ ^4P^o$	337.92
31	$2s^2 2p^5 3s(^3P^o)4d\ ^4F^o$	338.19
32	$2s2p^6 3s(^1S)3p\ ^2P^o$	338.70
33	$2s^2 2p^5 3s(^3P^o)4d\ ^4D^o$	338.71
34	$2s^2 2p^5 3s(^3P^o)4d\ ^2P^o$	339.25
35	$2s^2 2p^5 3s(^1P^o)4d\ ^2P^o$	341.39
36	$2s2p^6 3s(^3S)3p\ ^2P^o$	346.54
37	$2s2p^6 3s(^3S)3d\ ^4D$	361.24
38	$2s2p^6 3s(^3S)3d\ ^2D$	364.94
39	$2s2p^6 3s(^1S)3d\ ^2D$	367.23

III. RESULTS AND DISCUSSION

Electron-impact ionization cross sections for Ar^{7+} obtained by combining EA and REDA contributions to the direct-ionization cross sections are displayed in Fig. 1 as a function of electron energy between the $2s^2 2p^5 3s^2\ ^2P^o$ threshold at 248.63 eV and the $2s2p^6 3s(^1S)3d\ ^2D$ threshold at 367.23 eV. The present 45-state results are shown by the solid curve, the dotted curve represents the 19-state results, and the dashed curve gives the direct-ionization cross sections of Younger [18]. There are numerous Rydberg series of resonances of the types $2s^2 2p^5 3s3ln'l'$, $2s^2 2p^5 3s4ln'l'$, and $2s2p^6 3s3ln'l'$ converging to the various autoionizing states in this energy region. These resonances arise due to the REDA process. It should be noted that the 19-state calculation displays resonances up to the energy 294.09 eV, which is the excitation threshold for the highest autoionizing state $2s^2 2p^5(^3P^o)3d\ ^2P^o$ considered in this calculation. The resonances have been fully taken into account by calculating the inner-shell excitation cross sections at a very fine energy (0.068 eV) mesh. The cross sections are then convoluted with a 1.0-eV full width at half maximum. Our calculation shows a wealth of resonance structure due to the REDA process.

It is rather difficult to make a meaningful comparison between the two calculations because of the very complicated nature of the resonance structure. Though some of the peaks are larger in the 45-state calculation than in the 19-state calculation, it seems that many resonances have decreased in magnitude in the 45-state calculation, which perhaps can be attributed to the loss of flux in the additional $2s^2 2p^6 4l$ channels. However, our 45-state results

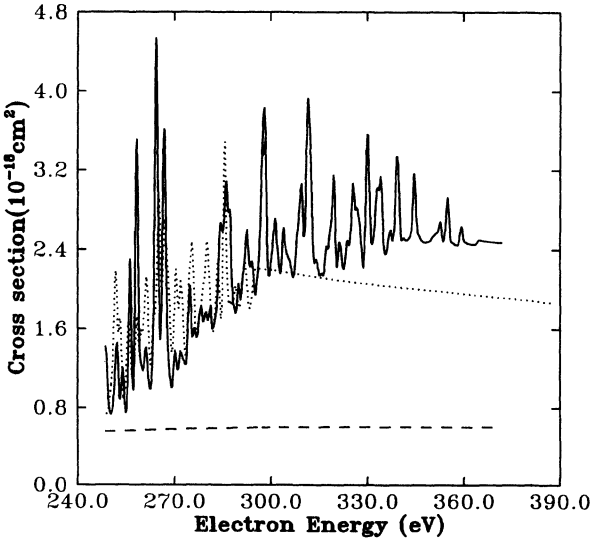

FIG. 1. Electron-impact ionization cross sections of Ar^{7+}. Solid curve, the present 45-state calculation; dotted curve, the present 19-state calculation; dashed curve, the direct-ionization cross section of Younger [18].

may still overestimate the REDA contributions as there is an infinitely large number of singly excited bound states $2p^6nl$ of Ar^{7+} to which the doubly excited states of Ar^{6+} can decay by single autoionization. Reed and Chen [21] found that $1s^2nl$ $(5 \leq n \geq 10)$ singly excited bound states for lithiumlike ions represent most important loss channels which reduce significantly the REDA contributions. In order to keep the size of present close-coupling calculations manageable, we did not test the effects of higher singly excited bound states $2p^6nl$ $(n \leq 5)$ on the resonance structure due to the REDA process. The inclusion of a large number of channels in the close-coupling expansions renders these calculations intractable. The distorted-wave methods are perhaps more appropriate to carry out such test calculations [21]. Above 294.09 eV, the $2s^22p^53s4ln'l'$ and $2s2p^63s3ln'l'$ Rydberg series of resonances contribute to the REDA process. It is clear from Fig. 1 that these series of resonances make significant enhancements in the cross sections. Similar enhancements in the cross sections by these intermediate states was noted by Chen, Reed, and Moores [3] for Fe^{15+}. The ratio of the total ionization cross section to the direct-ionization cross section fluctuates in this energy region. However, the ratio just above the highest threshold at 367.5 eV where the present calculation contains no REDA contribution is 4.2, which is lower than the distorted-wave calculation and the experimental value of Zhang *et al.* [9]. Zhang *et al.* [9] reported a calculated value of 5.4 and the experimental value of 5.3 ± 0.4 at 364 eV for Ar^{7+}.

In Fig. 2 we displayed the present 45-state calculation in the excitation threshold region together with the measured cross sections of Zhang *et al.* [9] and Rachafi *et al.* [10]. The present 45-state results are shown by the solid curve, and the solid and open circles give the measured values of Zhang *et al.* [9] and Rachafi *et al.* [10], respectively. The measured cross sections in this energy region are available only at a few energies and represent some fluctuations in cross sections. Detailed high-resolution measurements at a large number of energies are needed in this energy region to confirm the complicated resonance structure. The calculated results seem to agree with the measurements at the available energies. The sharp rise in the cross sections close to the $2p^53s^2\,^2P^o$ threshold is due to the EA indirect-ionization mechanism. The lowest three members of the $2p^53s3p(^4S)nl$ Rydberg series can be clearly seen in the energy region between 248.63 and 258.27 eV. The resonance structure for Ar^{7+} looks similar to that which we obtained for the isoelectronic Mg^+ ion except that some additional resonance features can be seen for Ar^{7+}.

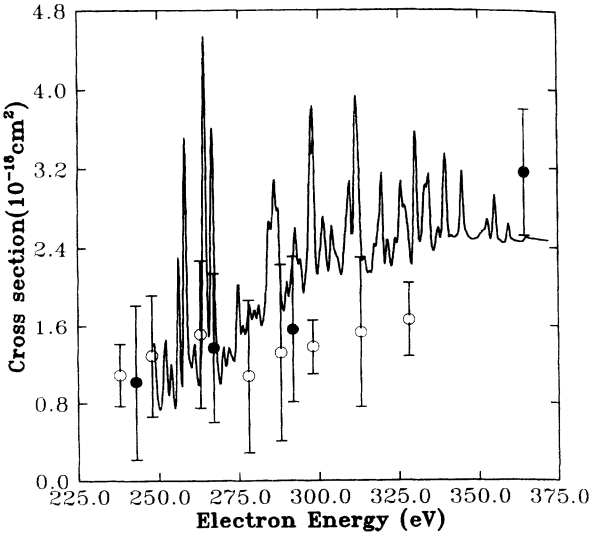

FIG. 2. Electron-impact ionization cross sections of Ar^{7+}. Solid curve, the present 45-state calculation; solid circles, the experimental values of Zhang *et al.* [9]; open circles, the experimental values of Rachafi *et al.* [10].

The total ionization cross sections calculated by adding

TABLE III. Inner-shell excitation cross section (10^{-18} cm^2) as a function of incident electron energies. Keys to the transitions are given in Table II.

	Electron energies (eV)		
Transition	390.0	440.0	489.0
1-2	0.0323	0.0304	0.0292
1-3	0.0191	0.0146	0.0115
1-4	0.0382	0.0290	0.0225
1-5	0.0159	0.0120	0.0092
1-6	0.0301	0.0281	0.0266
1-7	0.0102	0.0079	0.0062
1-8	0.0315	0.0272	0.0240
1-9	0.0219	0.0185	0.0159
1-10	0.0074	0.0058	0.0045
1-11	0.2723	0.2478	0.2278
1-12	0.0635	0.0467	0.0352
1-13	0.0597	0.0431	0.0319
1-14	0.0230	0.0159	0.0113
1-15	0.0695	0.0618	0.0565
1-16	0.5485	0.5604	0.5661
1-17	0.0084	0.0061	0.0045
1-18	0.0067	0.0064	0.0064
1-19	0.0361	0.0328	0.0298
1-20	0.0041	0.0029	0.0022
1-21	0.0061	0.0044	0.0033
1-22	0.0144	0.0104	0.0079
1-23	0.0058	0.0042	0.0031
1-24	0.0073	0.0066	0.0060
1-25	0.0048	0.0036	0.0027
1-26	0.0025	0.0018	0.0014
1-27	0.0070	0.0054	0.0043
1-28	0.0030	0.0023	0.0017
1-29	0.1063	0.0951	0.0866
1-30	0.0237	0.0173	0.0130
1-31	0.0245	0.0175	0.0128
1-32	0.0489	0.0555	0.0601
1-33	0.0115	0.0078	0.0055
1-34	0.0207	0.0174	0.0151
1-35	0.1209	0.1226	0.1221
1-36	0.0062	0.0051	0.0042
1-37	0.0334	0.0265	0.0205
1-38	0.0472	0.0522	0.0548
1-39	0.0157	0.0127	0.0099

the sum of inner-shell excitation cross sections to all autoionizing states from the ground state to the direct-ionization cross sections from the outer $3s$ subshell and inner $2p$ and $2s$ subshells are shown in Fig. 3 in the energy region from the $2s^22p^53s^2\,^2P^o$ threshold at 248.63 eV to 1000.0 eV. In order to demonstrate the relative importance of various autoionizing states included in the present 45-state calculation to the EA indirect process, we have listed in Table III the inner-shell excitation cross sections to the autoionizing states from the ground state at 390, 440, and 489 eV. The keys of the states involved in a transition are given in Table II. It is clear from this table that the $2s^22p^53s(^3P^o)np\,^2S$ and $2s^22p^53s(^3P^o)nd\,^2P^o$ ($n=3$ and 4) states make the largest contribution to the total indirect cross sections. As a matter of fact, these four states combined contribute 58% to the total indirect cross sections at 390 eV. The coupling effects are normally weak for most of the transitions in Ar^{7+} and may affect the total indirect cross sections by up to 5%. As the nuclear charge increases, it appears that the distorted-wave methods such as the one used by Chen, Reed, and Moores [3] for the isoelectronic Fe^{15+} and also for Li-like ions by Reed and Chen [21] should provide a reliable estimate for the indirect EA and REDA cross sections. The direct-ionization cross sections in the lower-energy region first decrease and then increase as the ionization thresholds of inner $n=2$ subshells are reached. The total ionization cross sections show a similar trend. The present results are smaller than the measurement of Zhang *et al.* [9] at incident electron energies above 390 eV, but are larger than the measurement of Rachafi *et al.* [10]. It should be noted that there is an infinitely large number of possible autoionizing states which may contribute to the total ionization cross sections in this energy region. We have only included a limited number of autoionizing states in our calculation to keep it manageable. The two experiments exhibit large differences in the cross sections, particularly at energies above 390 eV.

To summarize, we have calculated EA and REDA contributions in the electron-impact ionization of Na-like Ar^{7+}. Our calculation shows a wealth of resonance structure due to the REDA. The available measurements on electron-impact ionization of Ar^{7+} do not seem to have high resolution to detect these structures. Very clear experimental evidence for resonance structure is now available for the isoelectronic Mg^+ ions [6,7] and

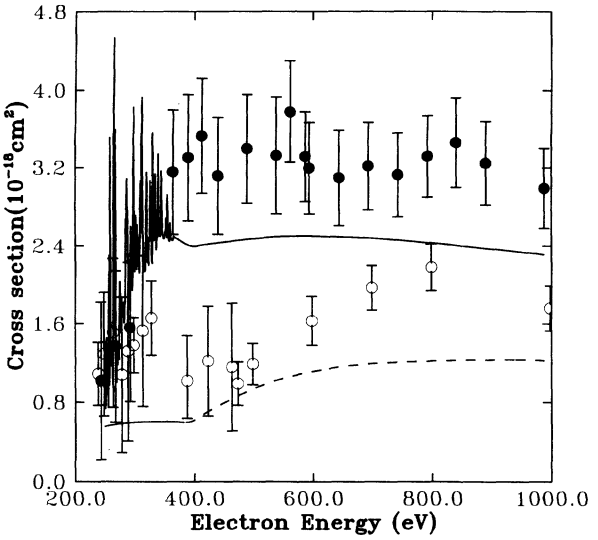

FIG. 3. Electron-impact ionization cross sections of Ar^{7+}. Notations are as in Figs. 1 and 2.

Li-like ions [22]. We hope our calculation will provide stimulus to the experimentalists to confirm the structure in cross sections. We included $2s^22p^53s3lnl'$, $2s^22p^53s4lnl'$, and $2s2p^63s3lnl'$ Rydberg series of resonances converging to the $2s^22p^53s3l$, $2s^22p^53s4l$, and $2s2p^63s3l$ autoionizing thresholds, respectively. The indirect processes typically contribute 25–30 % to the total ionization cross sections. Tayal and Henry [23] and Reed and Chen [21] in their work on the Li-like ions indicated that the autoionization of doubly excited states to singly excited bound states can reduce the resonance structure in the low-energy region. In order to account for loss of flux in these channels, we considered the $2p^6nl$ ($n=3$ and 4) singly excited states and ignored other higher excited states, which may introduce some errors in our results. We also have ignored relativistic effects and radiative decay of the autoionizing states in our work.

ACKNOWLEDGMENTS

This research is supported in part by the U.S. Department of Energy, Division of Chemical Sciences, and by the National Science Foundation. Generous supercomputer time on the NERSC supercomputers provided by the U.S. DOE, Fusion Energy, is appreciated.

[1] K. J. LaGattuta and Y. Hahn, Phys. Rev. A **24**, 2273 (1981).
[2] S. S. Tayal and R. J. W. Henry, Phys. Rev. A **39**, 3890 (1989).
[3] M. H. Chen, K. J. Reed, and D. L. Moores, Phys. Rev. Lett. **64**, 1350 (1990).
[4] K. A. Berrington, P. G. Burke, M. LeDourneuf, W. D. Robb, K. T. Taylor, and Vo Ky Lan, Comput. Phys. Commun. **14**, 367 (1978).
[5] D. C. Gregory, L. J. Wang, F. W. Meyer, and K. Rinn, Phys. Rev. A **35**, 3256 (1987).
[6] A. Muller, G. Hoffmann, K. Tinschert, B. Weissbecker, and E. Salzborn, Z. Phys. D **15**, 145 (1990).
[7] B. Peart, J. W. G. Thomason, and K. Dolder, J. Phys. B **24**, 4453 (1991).
[8] S. S. Tayal, J. Phys. B **24**, L219 (1991).
[9] Y. Zhang, C. B. Reddy, R. S. Smith, D. E. Golden, and D. W. Mueller, Phys. Rev. A **45**, 2929 (1992).
[10] S. Rachafi, D. S. Belic, M. Duponchelle, J. Jureta, M. Zambra, Hui Zhang, and P. Defrance, J. Phys. B **24**, 1037 (1991).
[11] D. L. Moores and H. Nussbaumer, J. Phys. B **3**, 161 (1970).
[12] R. D. Cowan and J. B. Mann, Astrophys. J. **232**, 940

(1979).
[13] D. C. Griffin, M. S. Pindzola, and C. Bottcher, Phys. Rev. A **36**, 3642 (1987).
[14] D. C. Griffin, C. Bottcher, and M. S. Pindzola, Phys. Rev. A **25**, 154 (1982).
[15] R. J. W. Henry and A. Z. Msezane, Phys. Rev. A **26**, 2545 (1982).
[16] D. H. Crandall, R. A. Phaneuf, R. A. Falk, D. S. Belic, and G. H. Dunn, Phys. Rev. A **25**, 143 (1982).
[17] E. D. Donets and V. P. Ovsyannikov, JINR Report No. P7-10780, 1977 (unpublished).
[18] S. M. Younger, Phys. Rev. A **24**, 1272 (1981).
[19] E. Clementi and C. Roetti, At. Data Nucl. Data Tables **14**, 177 (1974).
[20] A. Hibbert, Comput. Phys. Commun. **9**, 141 (1975).
[21] K. J. Reed and M. H. Chen, Phys. Rev. A **45**, 4514 (1992).
[22] G. Hoffmann, A. Muller, K. Tinschert, and E. Salzborn, Z. Phys. D **16**, 113 (1990).
[23] S. S. Tayal and R. J. W. Henry, Phys. Rev. A **44**, 2955 (1991).